

Spectral properties, electronic states, and aggregation of highly-fluorinated zinc phthalocyanines

Deborah Chan^{a,†}, Angel Zhang^{a,†}, Daisy L. Wong^{a,†}, Dennis Mercier^{a,†},
Marius Pelmuş^b, Hemantbhai H. Patel^b, Sergiu M. Gorun^{b,◊}
and Martin J. Stillman^{a,*◊}

^aDepartment of Chemistry, The University of Western Ontario, 1151 Richmond St., London, Ontario, N6A 5B7, Canada

^bDepartment of Chemistry and Biochemistry, Seton Hall University, 400 South Orange Ave., South Orange, NJ 07079, USA

Received 7 October 2025

Accepted 20 October 2025

Dedicated to the memory of Prof. A. B. P. Lever (Barry)

ABSTRACT: Fluoroalkyl zinc phthalocyanines (F_nPcZn) are an emerging class of functional tetrapyrroles with fluoro and perfluoroalkyl groups decorating the periphery of the macrocycle. F_nPcZn complexes, $16 \leq n \leq 64$, exhibit strong absorptivity in the red region of the visible spectrum. Analysis of absorption, emission, and, most importantly, magnetic circular dichroism spectra, coupled with detailed molecular orbital calculations using time-dependent density functional theory, was used to probe the differential effects of increasing the number of peripheral fluoro groups. The impact of the electronegativity imparted by the fluorine atoms and *iso* fluoroalkyl groups, as well as the resulting increased steric crowding, was considered in terms of the electronic properties of a range of porphyrins and phthalocyanines. The contribution of F_nPcZn aggregation to the electronic spectra in solution was elucidated by analyzing TD-DFT-calculated spectra and comparing them with the X-ray structure of the solid state.

KEYWORDS: time-dependent density functional theory, perfluorinated phthalocyanine, Gouterman 4-orbitals, substitution-induced splitting of HOMOs and LUMOs, magnetic circular dichroism.

INTRODUCTION

Fluorinated phthalocyanines (F_nPcs) and their metal complexes are a relatively recently developed class of electron-deficient, redox-stable, heat-resistant, singlet oxygen-producing tetrapyrroles [1–7]. Containing no C-H bonds, these robust, bioinspired materials include a combination of –F and bulky *iso*- C_3F_7 groups decorating the periphery of the macrocycle, which, along with a

variation in coordinated metals, (including Zn(II), Co(II), Cu, Fe, V=O, etc. or $2H^+$), drastically change their chemical and physical properties, as well as their catalytic and photocatalytic properties [8]. As a result, these molecules have found applications in water sterilization [9], thiol-coupling (relevant in the petroleum industry), C-P coupling [10], thin films [11, 12], advanced bioinspired sensors (replacing horseradish peroxidase) [13], coating materials [11, 12], and photodynamic therapy [14, 15]. Their photoactivity makes them excellent photosensitizers. In addition, they can replace oxygen-activating enzymes, being both redox stable and non-toxic.

Figure 1 summarizes the frontier π orbitals present for 18 π electron aromatic rings, focused on tetrapyrroles.

[†]SPP full member in good standing.

*Correspondence to: Martin J. Stillman, e-mail: martin.stillman@uwo.ca.

[◊]These authors contributed equally to this work.

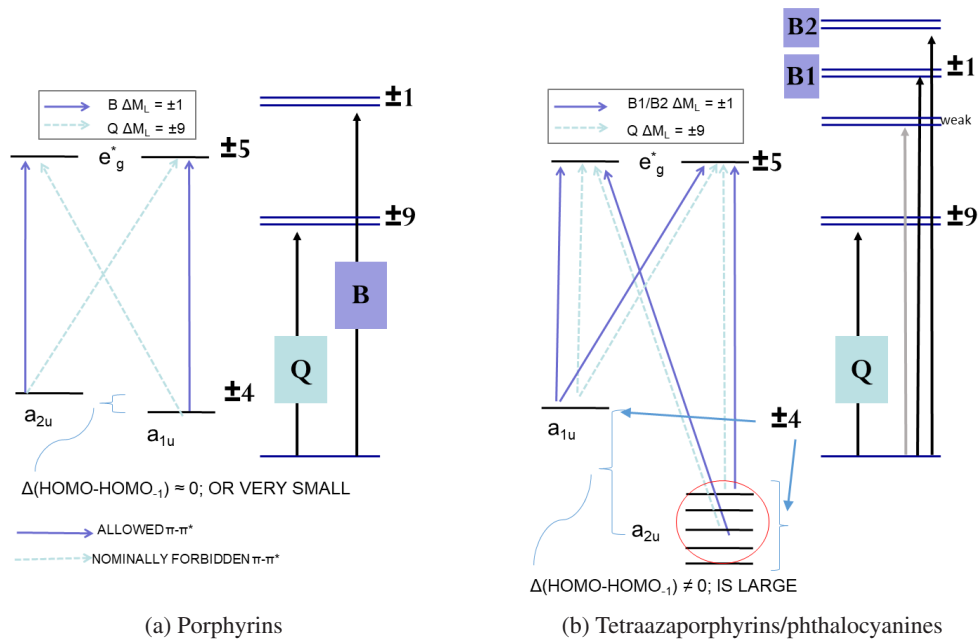


Fig. 1. The lowest energy states following Gouterman's four-orbital model. (a) In the porphyrin model, the HOMO and HOMO-1 orbitals have a_{2u} and a_{1u} symmetry, respectively. (b) In the tetraazaporphyrin/phthalocyanine model, the HOMO and HOMO-1 orbitals have a_{1u} and a_{2u} symmetry, respectively. Other occupied MOs between HOMO and HOMO-1 are shown as a series of energy levels [16–18].

The left-hand side (a) illustrates the traditional interpretation of the differences in molar absorptivity between the degenerate S1 state (the Q band) and the degenerate S2 state (the B band or Soret band).

Understanding the underlying electronic structure of the optical properties of all tetrapyrroles, and here of phthalocyanines, is critical for designing new complexes with specific applications in mind. So we take a moment here to summarize the key factors in the optical data, which we will report and discuss below for the fluorinated zinc phthalocyanines.

Using both theoretical results, and with many experimental examples, Martin Gouterman and his group explained why the Q band in porphyrins is very weak (because the angular momentum change of ± 9 breaks the selection rule of ± 1 or zero) and why transitions to the Soret band (a pair of states) is fully allowed and, therefore, observed as strong band in the 400 nm region (the angular momentum change is ± 1). The angular momenta thus control the structures of the excited states and determine the visible and UV-region spectra for all aromatic molecules [2, 16–20]. This is why MCD spectral data is so valuable for probing the electronic structure of tetrapyrroles in general. The transitions shown in Fig. 1, specifically for 18 π electron tetrapyrroles, include the forbidden S1 transition, which lies lower than the allowed S2 state. The angular momentum change, $\Delta(M_J)$ for S1, of ± 9 , precludes an optical transition, whereas for S2, which is an allowed $\pi-\pi^*$ transition, $\Delta(M_J)=\pm 1$ [21]. Vibronic overtone bands can significantly complicate

the actual observed spectra. The situation for tetraazaporphyrins is more complicated because the aza group differentially affects the two nominally degenerate highest occupied MOs. This is shown for metallophthalocyanines on the right-hand side of Fig. 1. This is the case for the fluorinated zinc phthalocyanines reported here. The systematic variations of the electronic properties of substituents can provide insights into their influence on the HOMO and HOMO-1 energies and the placement of the “HOMO-1” within the stack of occupied MOs, provided the metal center is kept constant. Among substituents, fluorinated substituents occupy a special place, as they impart steric and chemical robustness to the macrocycles to which they are attached, thereby enabling many technological and biomedical applications.

In this paper, we present detailed optical data for solutions of zinc phthalocyanines with peripheral substitutions of the 16 benzo-protons from 16 F up to the fully substituted 64 F using 8 *iso*-C(CF₃)₂(F) groups to increase the number of F per benzo unit to 16. The availability of UV-visible absorption, MCD, and associated emission and excitation spectra allows for the assessment of the effects of these withdrawing groups on the underlying electronic structures. In addition, we assessed the onset of dimerization. The complexes are abbreviated F₁₆Pc, F₄₀Pc, F₅₂Pc, and F₆₄Pc, respectively. The influence of the varying numbers of fluoro groups on the optical and photochemical properties of this class of functional fluorinated zinc phthalocyanines, F_nPcZn was probed using detailed molecular orbital energy calculations.

The fluorine-substitution-based trends revealed by these calculations explain the observed spectroscopic patterns arising from the ground and excited states. Significantly, we elucidate a trend in which the electron-withdrawing effect of fluorine is reflected in the appearance of several extra occupied MOs lying between the Gouterman-type HOMO and HOMO-1, a property that is not observable experimentally, but may have a significant experimental impact. The increasing energetic separation between the a_{1u} HOMO and the lower-lying a_{2u} "HOMO-1" is associated with a reduction in the % contribution of "HOMO-1" to the Q-band excited states, thereby increasing the oscillator strength of the Q band. TD-DFT calculations support the spectroscopic properties and proposed electronic structures reported here.

EXPERIMENTAL

Synthesis

Samples of F_nPcZn , $n=40, 52$ and 64 were synthesized as reported previously [4–7, 22]. $H_{16}PcZn$ and $F_{16}PcZn$ are commercially available.

Spectroscopy

Solvents were commercially available and used without further purification. DMF (Caledon) was used for all spectroscopic measurements. Absorption spectra were obtained on a Cary 50 UV-visible spectrophotometer (Varian, Toronto). MCD spectra were measured on a Jasco J-810 CD spectropolarimeter (Jasco, New Jersey) equipped with a 1.4 T magnet (Olis, USA). The solution emission and excitation spectra were recorded at 25 °C using a PTI Quanta Master scanning spectrofluorometer (London, Ontario). The same samples were used for measuring absorbance, MCD, emission, and excitation spectra.

Single-crystal X-ray structures were employed to analyze the formation of F_nPcZn dimers in the solid state using the Mercury software.

Computation methods

Preliminary structural models of F_nPcZn ($n=0, 16, 40, 52, 64$) were obtained by geometry optimization (GO) using molecular mechanics methods from the Scigress Software (Fujitsu, Poland). Molecular dynamics (MD) methods using the Scigress molecular modeling package (Fujitsu Poland), were used to refine the initial geometries, avoiding the formation of F-F bonds, which can be an issue when DFT methods are used before reasonable placement of the fluorine atoms has been established [23–25]. Subsequent optimizations were performed using the Gaussian 16 computational package [26] with the CAM-B3LYP functional and the 6-31G(d,p) basis set. No symmetry was imposed during the geometry minimization.

The SCRF parameter, including the Polarizable Continuum Model (PCM), was used for both geometry and excited-state calculations, selecting the default solvent, water. However, a test calculation selecting DMSO as a match for the DMF used for the spectroscopic measurements shown in Fig. 2 confirmed the results of Nemykin *et al.* [27], who found only slight differences in the dielectric constants of a range of solvents. The calculated IR frequencies (from the FREQ parameter) had positive energies, indicating that a stable stationary point had been reached. The energies of the 20 highest occupied and 20 lowest unoccupied MOs were retained and the molecular orbital surface properties were determined. Single point TD-DFT calculations at the level of CAM-B3LYP/6-31G(d,p) were carried out next, yielding the energies and MO contributions to the lowest 100 excited states. Gauss View 6 was used to calculate the theoretical absorption spectra, setting the band halfwidth at 250 cm⁻¹ for the Q band and 800 cm⁻¹ for the UV region bands to more closely match the experimental spectra. TD-DFT calculations, even with the CAM-B3LYP hybrid functional, generally overestimate the energy of the lowest excited states of tetrapyrroles. Using the PCM solvent (water), however, red-shifts the Q band by 10–30 nm, thus reducing the overestimate of the S1 state energy to ~100–200 cm⁻¹ blue-shifted relative to the experimentally determined value.

RESULTS AND DISCUSSION

The monomeric species: Experimental and theoretically-calculated spectra

The increase in the number of F's at the periphery of the $PcZn$ molecule probes the sensitivity of the aromatic ring MOs, and thus the associated optical spectra. The substitution of F with R_f groups affects both the optical and redox properties of $PcZn$, as well as its symmetry (Fig. 2).

The absorption spectra in DMF are typical of $PcZn$ complexes, with a Q-band absorbance much greater than the B-band absorbance observed in the 300–400 nm region (Fig. 2) [2, 28]. The spectroscopic and MCD data obtained in solution need to include the possibility of the formation of Pc dimers, in equilibrium with the monomers. The emission and excitation data are essential for determining the precise band maxima wavelengths because, while the monomers emit, the predicted H-dimers (assuming the π–π stacking interactions of the solid state hold in dilute solution) do not [29]. Interestingly, given the close overlap between the excitation spectra and the predicted monomeric absorption profile, we suggest that the low fraction of aggregates observed in the solutions used in Fig. 2 is indeed an H-dimer involving π–π stacking interactions. The MCD data clearly show the presence of mixtures of monomers and dimers

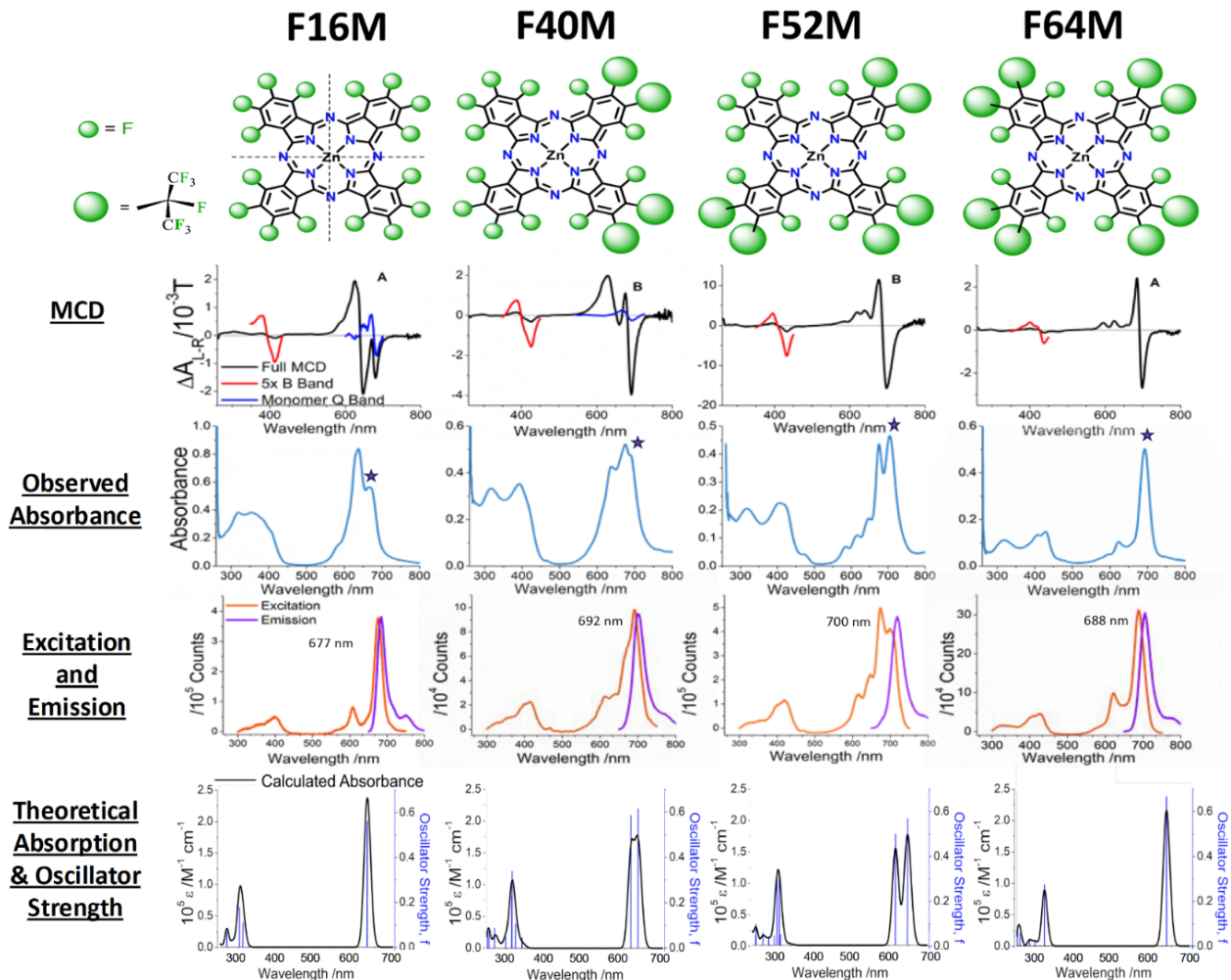


Fig. 2. A composite of MCD, absorption, and emission spectroscopic data for monomeric (M) F_n PcZn in DMF and TD-DFT calculated absorption spectra. 1st row: F_{16} – F_{64} PcZn structures. Aromatic F and *iso*- C_3F_7 groups are represented by smaller and larger spheres, respectively. The remaining atoms are shown as capped sticks. The four quadrants of Pcs are defined explicitly for the F_{16} PcZn structure. In the second row: MCD spectra. The B bands (intensity expanded 5x) are shown in red; the monomer Q bands are shown in blue. The A or B next to the Q band denotes the Faraday term. 3rd row: UV-visible absorption spectra. 4th row: excitation spectra (red trace) and the emission spectra (purple trace), with the monomeric Q band centers added. The excitation band maxima identify the monomer's Q_{00} band for F_{16} PcZn at 677 nm; F_{40} PcZn at 692 nm; F_{52} PcZn at 700 nm; and F_{64} PcZn at 688 nm. 5th row: TD-DFT calculated absorption spectra for the monomeric complexes (black trace), their associated oscillator strengths (blue trace) on the right-hand y-axis. Band broadening was applied to the Gaussian stick data: 800 cm^{-1} for 200 – 500 nm and 250 cm^{-1} for 500 – 750 nm. Note that the x-axes of the calculated data are red-shifted with respect to the experimental data in rows 3 and 4 by approximately 50 nm to line up the Q and B1 bands. The TD-DFT stick representation of the oscillator strengths in Table 1 is shown in Fig. S1.

in the overlapping A terms. The MCD A term magnitudes can be quantified approximately by comparing the A/D values [30] using the $\Delta(M_j)$ magnitude and the absorbance of the same solution at that wavelength. The presence of the nominal $\Delta(M_j)$ of S1 of ± 9 and for S2 of ± 1 , results in the noticeable 9:1 difference in MCD spectra. We should, at this point, change our nomenclature, because while the Gouterman analysis of tetrapyrroles (Fig. 1(a)) assigns S1 and S2 as two degenerate states, for azaporphyrins (and here, the phthalocyanines), the Q band should be considered as a pair of states — S1 and S2 — and the B band as S3 and S4. And that is how

we have set up in Table 1, which summarizes our spectral and theoretical analyses. The TD-DFT program actually only provides the energies and oscillator strengths of transitions to excited states; the band-broadened profiles are from, in our case, the GaussView 6 program. We have plotted the stick with broadened band profiles in Fig. S1, as the extra information from the stick representation is contained in Table 1, but also complicates the visual effect in Fig. 2.

The calculated UV-visible absorption spectra in Fig. 2 match the solution data the best for $n=52$ and 64, the least likely F_n PcZns to aggregate. Such dimers, part of

Table 1. Experimental and calculated energies of the monomeric complexes.

Compound	Experimental Q band (nm)	State	Q band State Energy (nm)	Oscillator Strength (f)	Transition		% Orbital contributions
					HOMO, LUMO		
$H_{16}PcZn^a$	670 ^a	S1 Q_{-1}	623	0.62	146 → 149	3.7	
					147 → 148	73.6	
		S2 Q_{+1}	623	0.62	147 → 149	21.5	
	677	S1 Q_{-1}	632	0.66	146 → 148	3.7	
					147 → 148	21.5	
		S2 Q_{+1}	632	0.66	147 → 149	73.6	
$F_{16}PcZn$	692	S1 Q_{-1}	635	0.75	208 → 213	4.4	
					211 → 212	94.7	
		S2 Q_{+1}	617	0.71	208 → 212	4.4	
	700	S1 Q_{-1}	647	0.82	211 → 213	94.7	
					353 → 357	3.7	
		S2 Q_{+1}	617	0.72	353 → 356	3.8	
$F_{52}PcZn$	688	S1 Q_{-1}	636	0.80	355 → 357	94.8	
					425 → 429	2.9	
		S2 Q_{+1}	636	0.80	427 → 428	94.9	
	692	S1 Q_{-1}	647	0.82	425 → 428	3.3	
					427 → 429	94.4	
		S2 Q_{+1}	617	0.72	498 → 501	5.0	
$F_{64}PcZn$	692	S1 Q_{-1}	636	0.80	499 → 500	92.0	
					499 → 501	2.4	
		S2 Q_{+1}	636	0.80	498 → 500	5.0	
	700	S1 Q_{-1}	647	0.82	499 → 500	2.4	
					499 → 501	92.0	

^aExperimental data from Nyokong *et al.* [28] for ZnPc in DMSO.

the structural variations observed in the examined molecules, are indeed present in the solid state, as evidenced by the X-ray diffraction results (Fig. 3).

Geometric structural considerations are the basis for understanding electronic structures. The aromatic F_nPcZn rings are planar when the metal is 4- or 6-coordinated, as seen in the X-ray structures (Fig. 3) [14, 32]. The rotational symmetry of the complexes varies with n. A 4-fold rotational axis is present in $H_{16}PcZn$ and $F_{16}PcZn$ and both have D_{4h} symmetry. The symmetry effects of the R_f groups must be considered in terms of their impact on the overall electronic structure of the Pc. The location of the R_f groups, like those of the aromatic F, is in the molecular plane, irrespective of the rotational orientation of the F and CF₃ of *iso-C₃F₇*. This could be viewed as a single, bulky, pseudo aromatic atom with σ no π electronic effects. Thus, C₄ and σ symmetry

operations are present in $F_{64}PcZn$, *i.e.* a nominal D_{4h} symmetry. The exact approximation introduces mirror planes in the $F_{40}Pc$ and $F_{52}Pc$ scaffolds, which have C_{2v} point group symmetry. In the case of 5-coordination, the Zn is located slightly above the Pc plane, which may become convex, reducing the D_{4h} symmetry to C_{4v}. An increase in coordination numbers from 4 to 6 (5 is less likely in solution) may occur in coordinating solvents, such as DMF. In general, for the coordination number 6, the metal is in the Pc plane.

Figure 3 shows the solid-state structures that will guide our interpretation of dimer formation in solution using DFT methods. The $H_{16}Pc$, $F_{16}Pc$, $F_{40}Pc$, and $F_{52}Pc$ scaffolds aggregate via π interactions of the Pc quadrants that do not bear R_f groups, namely 4, 2, and 1. The solution supramolecular behavior of F_nPcZn parallels their solid-state properties.

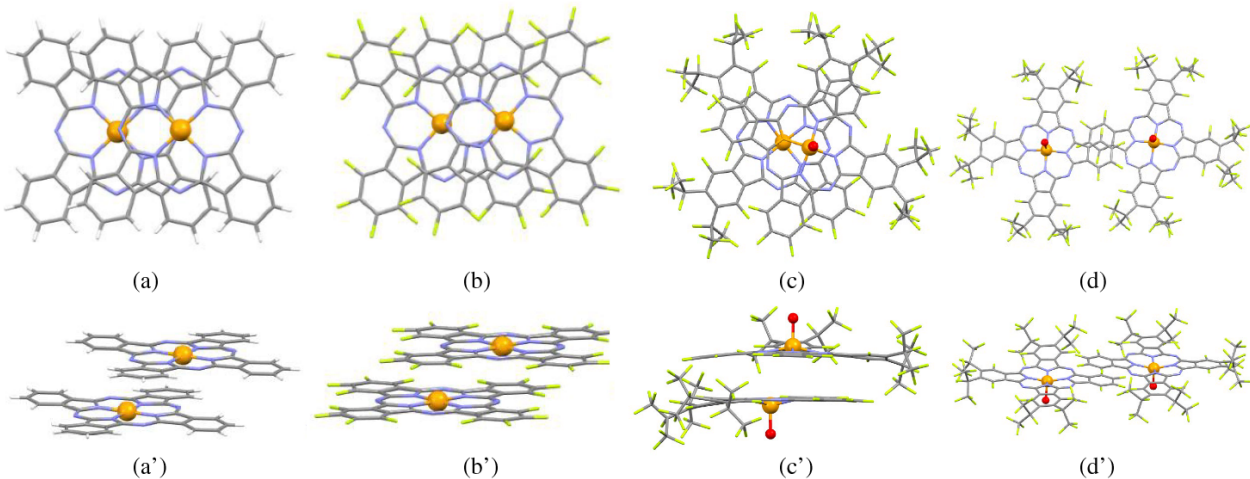


Fig. 3. Single-crystal X-ray structures of the F_nPcZn scaffold, $n=0, 16, 40$ and 52 . All atoms, except the metal centers, are represented as capped sticks. The X-ray structures of $F_{40}PcZn$ [7] and $F_{52}PcZn$ [6], while their synthesis has been previously reported, have not been published or submitted to the database. These two structures are being reported here for the first time, and their structural parameters have been submitted (Supplementary statement). For $F_{40}PcZn$ and $F_{52}PcZn$, only the oxygens of their triphenylphosphine oxide axial ligands are shown to reveal the C_{4v} coordination spheres. The dimer assembly is governed by π - π stacking interactions and other packing forces. Color codes: Zn, orange; F, green; C, black; N, blue; O, red; H, white. (a) and (a') $H_{16}PcZn$, front and side views, respectively; (b) and (b') $F_{16}PcZn$, front and side views, respectively; (c) and (c') $F_{40}PcZn$, front and side views, respectively; (d) and (d') $F_{52}PcZn$, front and side views, respectively. The structure of $H16$ (a, a') was redrawn with coordinates from Scheidt and Dow [31] and the structure of $F16$ (b, b') was redrawn with coordinates from Jiang *et al.* [32].

We used the concentration trend to track the development of dimer formation in a solution of $F_{16}PcZn$, as shown in Fig. 4. Separately, we used chloroform and ethanol to form the pure monomers and dimers, respectively (Fig. 4). Typically, a common solvent is DMF, but there is the possibility of mixtures of monomers with unknown dimer fractions. Because of vibronic overtone bands, assessing the fraction of dimers can be difficult. We also used the calculated spectra of the monomers and dimers (*vide infra*) to synthesize the spectra in DMF, demonstrating the power of theoretical data in assessing optical spectra.

Theoretical calculations help explain the observed spectral features. The energies of the occupied and unoccupied orbitals for monomeric species are shown in Fig. 5. Figure 6 shows the major transitions leading to the Q-band pair of states (S1 and S2).

The MOs that participate in the S1 and S2 transitions are shown in Fig. 6. The π - π^* orbitals with $+/-4$ and $+/-5$ angular momenta are easily identified from the nodal patterns. The calculations for monomeric species rationalize the noticeable split in the Q band of $F_{52}PcZn$.

Table 1 collects the experimental and computational results for the introduction of F at the periphery of Pcs, which can be placed in the context of previously established linear correlations between the strength, energy, and wavelength of Q-bands' oscillators, *vs.* calculated Δ HOMO, HOMO-LUMO gap, and wavelengths, respectively. The linear correlations included both porphyrins and phthalocyanines, as shown in Fig. 8 (Zhang *et al.* [1]), with data from Mack *et al.* [21].

Table 1 summarizes the experimental optical data and the associated oscillator strengths, orbital transitions, and their relative fractional contributions to Q bands from the TD-DFT calculations. The MO contributions to the pair of Q band states are presented to indicate Gouterman's highest and lowest occupied MOs, respectively.

The dimeric species: Experimental and theoretically-calculated spectra

The calculated electronic properties for the F16 and F40 dimers are shown in Fig. 7, with the individual transitions to each state shown in Table 2. It is interesting to us that for F40, the “lopsided” distribution of F's meant that the lowest energy dimer from the geometry minimization had the two rings staggered oppositely. There is a single transition to S3 with an exceptional oscillator strength (1.172) that spans MOs 702–714 — a movement of charge from the periphery to the core. This transition would not exhibit an MCD profile because the S3 state is clearly nondegenerate.

These extensive theoretical calculations confirm that electron-withdrawing groups reduce electron density on the Pc ring, thereby lowering the energy of the frontier orbitals. The symmetry reduction also changes the MO energies. Both factors affect the Δ (HOMO–HOMO-1) energies that almost linearly correlate with the oscillator strength of Q bands [21]. The presence of aggregation, even at low concentrations, is evident from broadened or even doubled Q bands (Fig. 2).

The orbital pictures and associated transitions for the dimers are shown in detail in Figs. 5 and 6. Our calculations

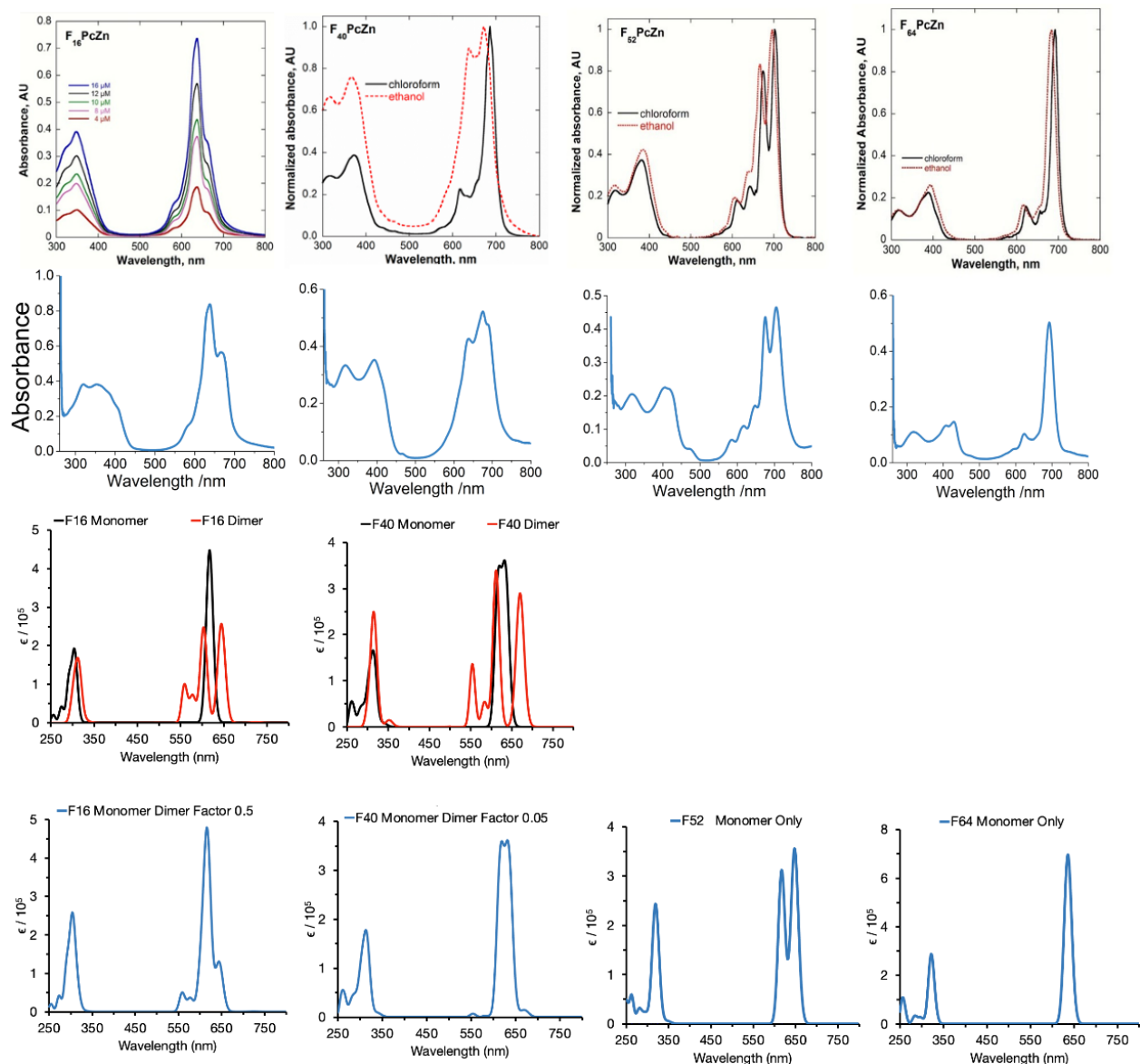


Fig. 4. Analysis of the aggregation of the $F_n\text{PcZn}$ species in solution. 1st row: (Left) observed spectra for the monomer/dimer fraction of $F_{16}\text{PcZn}$ as a function of concentration, and (Right) the solvent dependence of the monomer/dimer fraction of $F_{40}\text{PcZn} - F_{52}\text{PcZn} - F_{64}\text{PcZn}$ using ethanol and chloroform. 2nd row: experimental spectra (from Fig. 2), at room temperature, measured in DMF. 3rd row: overlay of the monomer (black) and dimer (red) calculated spectra for $F_{16}\text{PcZn}$ and $F_{40}\text{PcZn}$. 4th row Analysis of the experimental spectra in row 2 based on a factor-determined mix of the monomer and dimer computed spectra.

of the dimers, carried out at the same level as for the monomers, account for electronic transitions, and such assignments appear to be previously unreported (Fig. 7).

It should be noted that aggregation is solvent dependent. Hydrophobic solvents, such as CHCl_3 , stabilize monomers, whereas aggregation is enhanced in ethanol (Fig. 4) [33, 34]. The emission and related excitation data (row 4 of Fig. 2) are typical of “mirror-image” spectra of Zn-phthalocyanines and confirm that they are monomer spectra. Dimeric phthalocyanines do not emit strongly due to nonradiative pathways. However, the excitation spectra show band broadening due to the low symmetry of $F_{40}\text{PcZn}$ and $F_{52}\text{PcZn}$.

In contrast, $F_{16}\text{PcZn}$, while exhibiting aggregation, is a symmetric complex. Thus, there is no band broadening in the excitation spectra, even though the absorption and MCD spectra (see below) are dominated by band broadening effects. $F_{64}\text{PcZn}$ exhibits no band broadening, indicating a lack of aggregation and symmetry-lowering effects. The excitation maxima have been used to identify the monomeric band centers and thus the monomeric Q bands’ contributions to the absorption spectra. The full results are listed in Table 1 above.

In Fig. 8, we observe a common trend: on the scale of the graphs, the fluorinated Pcs are clustered above the linear correlation line. Specifically, the Q bands of

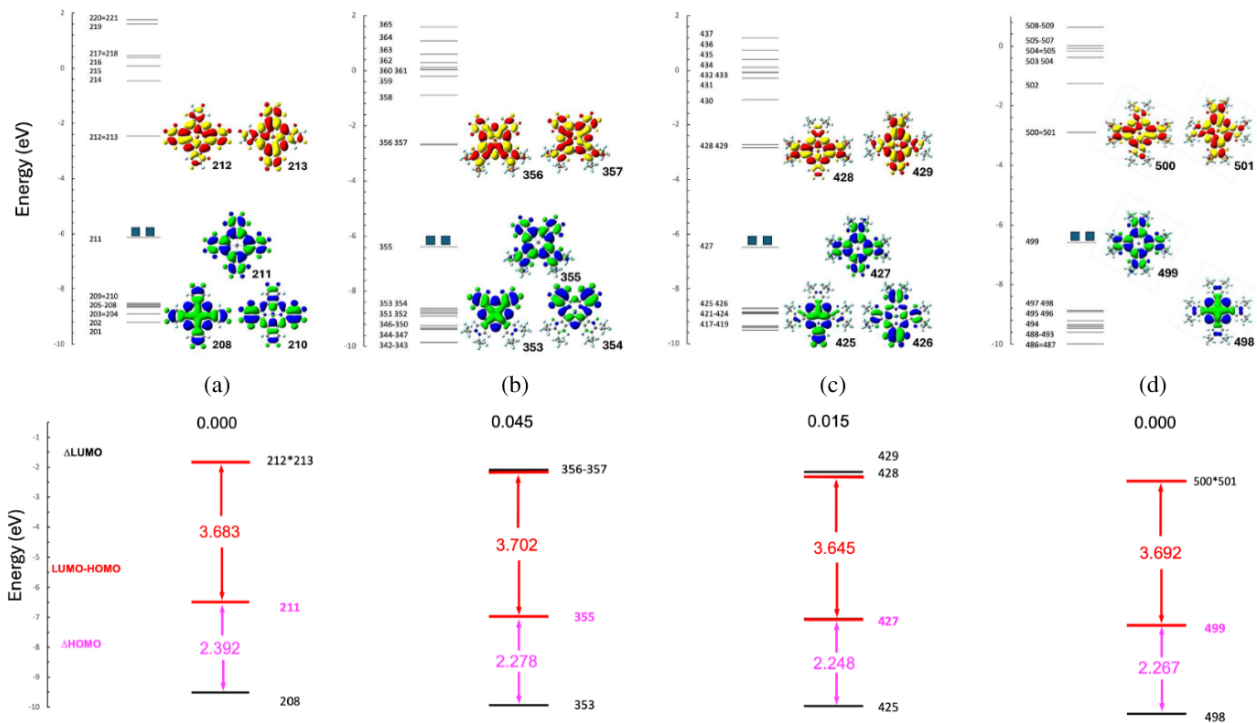


Fig. 5. Top row. Highest occupied and lowest unoccupied MOs for (a) F₁₆PcZn, (b) F₄₀PcZn, (c) F₅₂PcZn and (d) F₆₄PcZn. Two squares indicate the HOMO. The surfaces for the occupied MOs shown are blue and green, and they include both the HOMO and “HOMO-1,” together with the occupied MO identified by TD-DFT calculations as contributing to the S1 excited state. The surfaces for the LUMO pair of orbitals are also shown as red and yellow. Bottom row: Orbital energy differences (in eV) between the four Gouterman orbitals identified by the TD-DFT calculations. The nominal Gouterman “HOMO-1” orbital is determined by its nodal pattern, so there may be additional occupied MOs between the HOMO and “HOMO-1”. The HOMO and LUMO are shown in red, with the orbitals that give rise to the excited-state transitions. The values of the corresponding Δ HOMO–LUMO are indicated and labelled with the corresponding color.

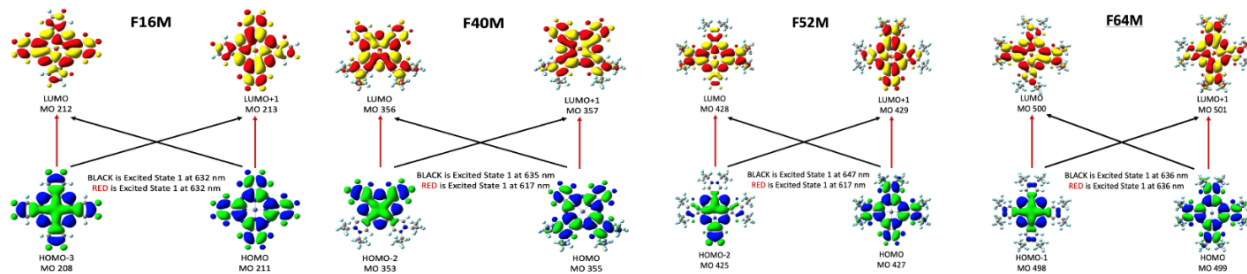


Fig. 6. Top row: MO transitions that contribute to the monomeric Q band for F₁₆PcZn, F₄₀PcZn, F₅₂PcZn and F₆₄PcZn. Black and red lines represent transitions that contribute to the Q₋₁ (S1) and Q₊₁ (S2) excited states, respectively.

the fluorinated Pcs are more red-shifted than the calculations predict, even when the solvent is included. Still, they exhibit extreme intensities that are stronger than the calculated values. Interestingly, the Δ (HOMO–HOMO-1) is relatively constant, indicating that HOMO-1 with its a_{2u} symmetry is insulated from the electron-withdrawing effects on the benzo rings.

For most tetrapyrroles, Gouterman’s model generally assumes degenerate LUMO and LUMO+1 [1, 30]. Peripheral substitutions result in quite extensive changes to the “ a_{2u} ” orbital, which is always far below

the “ a_{1u} ” highest occupied orbital in tetraazaporphyrins. The observed MCD spectra in Fig. 2 are a composite of the monomer and dimer species, with the dimer intensity lying to higher energy. In addition, as noted above, the excited state of each complex may be split by symmetry effects. In each case, the MCD spectral profile will change in sign (-) to (+) on going from low energy to high energy or high wavelength to low wavelength, from the Q band towards the B bands. Both the monomers (M) and dimers (D) exhibit the same (-)/ (+) sequence, since the change in angular momentum

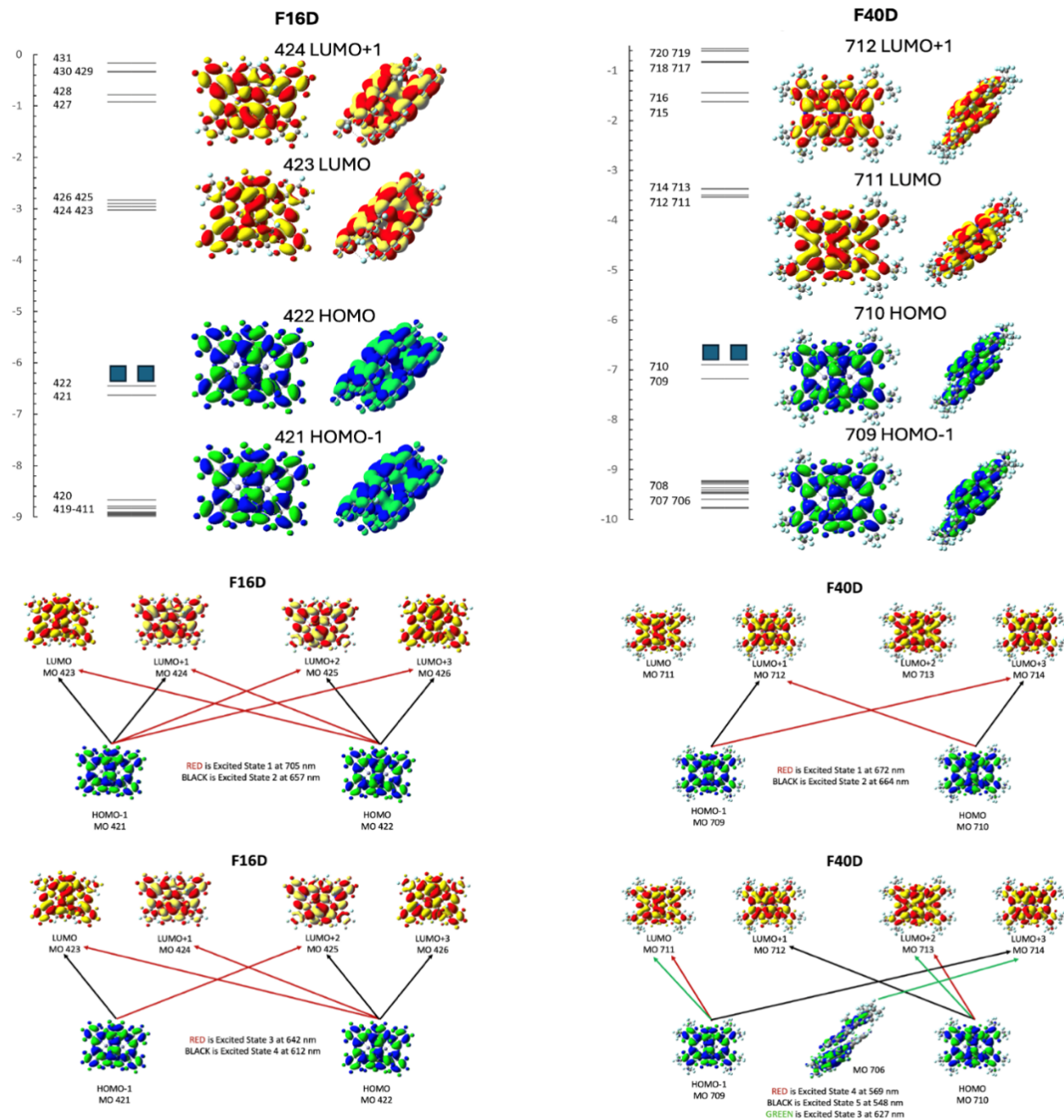


Fig. 7. Molecular orbitals and electronic transitions calculated for F_nPcZn dimers (D), n=16 and 40. Top panel: Highest occupied and lowest unoccupied MOs for F₁₆PcZn, and F₄₀PcZn, paired with a side-on view for clarification of the dimer structure. Two squares indicate the HOMO. The surfaces for the occupied MOs shown are blue and green, and they include both the HOMO and “HOMO-1,” together with the occupied MO identified by TD-DFT calculations as contributing to the S1 excited state. The surfaces for the LUMO pair of orbitals are also shown as red and yellow orbital origins of the Q bands. Lower panel: *intra*-dimer electronic transitions from the TD-DFT calculations summarized in Table 2. MO transitions that contribute to the dimeric Q bands (S1, S2, S3 and S4) for F₁₆PcZn, and F₄₀PcZn. Black and red lines represent transitions contributing to the Q₋₁ (S1) and Q₊₁ (S2) excited states, respectively, as well as the paired transitions due to the dimer for the Q₋₁ (S4) and Q₊₁ (S5) excited states. A charge-transfer state (S3) is shown, identified by green lines.

is positive, meaning it is lower in the ground state and greater in the excited state.

Using the crossover wavelength of that spectrum allows one to align the shoulders in the absorption spectrum and the peak in the excitation spectra as the monomer

spectrum. The MCD spectra indicate that dimers dominate F₁₆PcZn and F₄₀PcZn. In contrast, F₅₂PcZn and F₆₄PcZn show only a low dimer fraction. These findings agree with the UV-visible absorption data and the solid-state structural patterns observed (Fig. 3). Moreover, the

Table 2. The MO transitions calculated for the Q band region states in the dimeric F₁₆PcZn, and F₄₀PcZn.

Dimers Compound	State	Q band State Energy (nm)	Oscillator Strength (f)	Transition	% Orbital contributions
F ₁₆ PcZn D	S1 Q ₋₁	704	0.0077	421 → 425	3.6
				421 → 426	12.4
				422 → 423	72.3
				422 → 424	8.8
	S2 Q ₊₁	657	0.0013	421 → 423	6.8
				421 → 424	23.0
				422 → 425	53.7
				422 → 426	12.3
	S3 Q ₋₁	642	0.967	421 → 425	6.8
				422 → 423	20.1
				422 → 424	53.7
	S4 Q ₊₁	612	0.961	421 → 423	45.1
				422 → 425	17.2
				422 → 426	29.6
F ₄₀ PcZn D	S1 Q ₋₁	672	0.946	709 → 714	6.1
				710 → 712	89.3
	S2 Q ₊₁	664	0.013	709 → 712	21.7
				710 → 714	73.6
	S3 CT	627	1.172	706 → 714	2.2
				709 → 711	29.6
				710 → 713	64.5
	S4 Q ₋₁	569	0.032	709 → 711	66.0
				710 → 713	31.7
				709 → 714	90.0
	S5 Q ₊₁	548	0.302	710 → 712	7.4

symmetry-induced splitting of the monomeric Q band (Q-/Q+) occurs because the A term, or pseudo-A term (from the two B terms of opposite sign) is both symmetric and very close to the crossover point. Indeed, our MCD spectral data for PcZn(CN)₂ (not shown) gives a peak-to-trough span of only 11 nm. This represents the spectral profile of an A term that implies that the main component to the splitting of the Q-/Q+ components originates only from the applied magnetic field.

Band broadening and structural effects for the F_nPcZn complexes studied here would be expected to result in broader bands, even when no symmetry-lowering is present. That said, the MCD spectra in the Q-region span 14 nm for F₁₆PcZn and F₆₄PcZn, and this may be associated with the zero splitting of Q-/Q+ in the theoretical analysis. For the nonsymmetric complexes, the

comparison between the experimental data and theoretical data is as follows: F₄₀PcZn: 24 nm (18 nm); F₅₂PcZn: 29* nm (31 nm). (*The absorption data exhibit band maxima at 675 and 704 nm, indicating that the MCD spectral envelope, in this case, is still overlapped by the dimer bands, and so the absorption data are used.) The average difference is 4 nm, which is quite remarkable and within experimental error, confirming that, as in a previous analysis of low-symmetry phthalocyanines, the theoretical analysis can match the small symmetry-lowering changes that peripheral substituents impart to the π ring.

Summarizing, analysis of the MCD spectral data from trough to peak for the F_nPcZn complexes compared with the values for (CN)PcZn {trough(-), crossover, peak(+)} nm are as follows: F₁₆PcZn MCD span=14 nm {682 nm, 675 nm, 668 nm}, theoretical 0 nm {632–632} nm;

$F_{40}\text{PcZn}$ MCD span=24 nm {692 nm, 680 nm, 668 nm}, theoretical 18 nm {635 nm – 617 nm}; $F_{52}\text{PcZn}$ MCD span=22 nm {699 nm, 686 nm, 677 nm}, theoretical 31 nm {647 nm – 617 nm}; $F_{64}\text{PcZn}$ MCD span=14 nm {698 nm, 691 nm, 684 nm}, theoretical 0 nm {636 nm – 636 nm}; (CN) PcZn MCD span=11 nm {679 nm, 673 nm, 668 nm}, theoretical 0 nm {623 nm – 623 nm}.

The experimentally determined reduction in frontier orbital energies could justify the preferred anionic forms of these ZnPcs [35–37]. Interestingly, in addition to Cl^- adducts noted *via* the mass spectrometry (negative modes) of neutral molecules, we have recently reported

$[\text{F}_{64}\text{Pc}(-3)\text{Cu(II)}]^{+1}$ and $[\text{F}_{64}\text{Pc}(-4)\text{Cu(II)}]^{+2}$ complexes [38]. The location of not only the first extra electron, but also the second one on the F_{64}Pc ligand, in the presence of the $3d^9$ metal that could have been reduced was surprising, but consistent with the prior experimental and theoretical findings, including those reported here.

Figure 8 summarizes the optical and theoretical properties of these highly fluorinated complexes. To our surprise, we find that even the extreme electron-withdrawing nature of the 64 F's does not dramatically change the optical properties of the ZnPc ring. The previous report by Keizer *et al.* [23], demonstrating high stability for the reduced F_{64}ZnPc , shows that the very slight reduction in the HOMO energy is sufficient.

CONCLUSIONS

The spectral data and theoretical background for the excited-state properties of four perfluorinated zinc phthalocyanines, those with 16, 40, 52, and 64 fluorine atoms, are reported. The wide range of increasing inclusion of powerful electron-withdrawing groups from the symmetric F_{16} , with each of the four benzo protons replaced with F, to the symmetric F_{64} , provides an excellent structural basis which to explore the systematic change that takes place as the aromatic core is depleted of electron density in small steps.

Three properties connect the optical spectra to the theoretical analysis of electronic structures, as highlighted in Fig. 8. This Figure is then a compact summary of the results of the calculations and the experimental data.

First, the presence of fluorines significantly increases the oscillator strength compared with the nonfluorinated phthalocyanine “ H_{16}Pc ”. The trend clearly illustrates the effect of growing electron-withdrawing effects on the optical transition, even though the $\{\text{(HOMO)}-\text{(HOMO-1)}\}$ energy remains constant. The second trend compares the HOMO-LUMO energy with the Observed Q band energy. Now there is little change across the different fluorination levels, indicating that both the HOMO and LUMO energies decrease together, a trend seen in Fig. 6. Finally, the third trend, comparing the calculated and observed Q band energies, suggests that the oscillator-strength trend is mirrored in the Q band energies.

As far as we know, no theoretical data on phthalocyanine dimerization have been reported at the same level as the monomer, allowing consistent comparison. In this instance, we reproduced the dimer-induced splitting of the Q band, enabling us to match the observed data with the theoretically predicted data.

Acknowledgments

Natural Sciences and Engineering Research Council of Canada Discovery Grant (00037-2015; 06545-2020) to MJS, and Queen Elizabeth II Ontario Graduate Scholarships to DLW and AZ are gratefully acknowledged. Dr. R. Lalancette, USA, is thanked for the F_{40}PcZn and

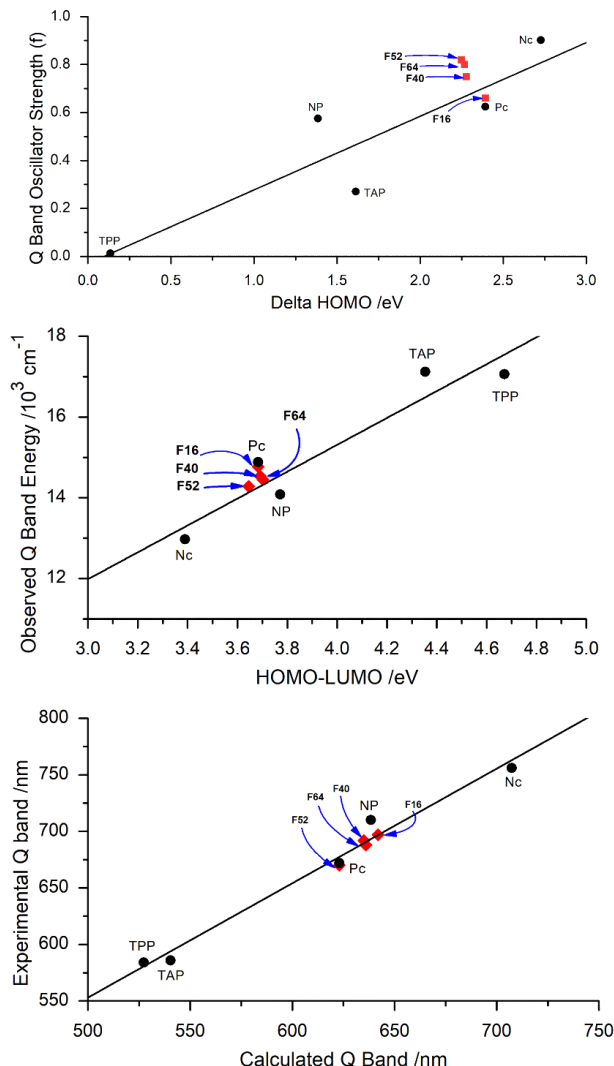


Fig. 8. Trends connecting experimental and calculated data. The F_nPcZn data are identified by red diamonds. Trends connecting the experimental and calculated data of other porphyrins and Pcs with the fluorinated Pcs described here. Graphs adapted from Zhang *et al.* [1] with data from Mack *et al.* [21]. (Top) Q-band oscillators strength vs. HOMO; (Middle) Q-band energy vs HOMO-LUMO gap; and (Bottom) Observed Q band vs. calculated Q-band energy. The compounds are as follows: tetraphenylporphyrin (TPP), naphthaporphyrin (NP), tetraaza-porphyrin (TAP), phthalocyanine (Pc), naphthalocyanine (Nc).

$F_{52}PcZn$ X-ray data. J. Vanstone is thanked for long-standing, outstanding instrumental support at the UWO. The National Science Foundation (Award 1448869) is thanked for support to SMG at SHU.

Supporting information

Figure S1 shows the stick representation of the excited state transitions calculated in the TD-DFT program and realized by the Gauss View 6 program, for the monomeric species in Fig. 2, and are included in the supplementary material, which is available free of charge online at <http://www.worldscientific.com/doi/suppl/10.1142/S1088424625501093>.

The full X-ray structures used to extract the architecture of fluorinated Pcs dimers, $F_{40}PcZn$ and $F_{52}PcZn$. While the structures contain $(Ph_3)P=O$ as axial ligands, the MCD samples do not. Crystallographic data have been deposited at the Cambridge Crystallographic Data Centre (CCDC) under the numbers CCDC-2493345 and 2480410. Copies can be obtained on request, free of charge, via <https://www.ccdc.cam.ac.uk/structures/> or from the Cambridge Crystallographic Data Centre, 12 Union Road, Cambridge CB2 1EZ, UK (fax: +44 1223-336-033 or email: deposit@ccdc.cam.ac.uk).

REFERENCES

- Zhang A and Stillman MJ. *Phys. Chem. Chem. Phys.* 2018; **20**: 12470–12482.
- Zhang A and Stillman MJ. Handbook of Porphyrin Science with Applications to Chemistry, Physics, Materials Science, Engineering, Biology and Medicine: Phthalocyanine Synthesis and Computational Design of Functional Tetrapyrroles. Vol 45. Eds. (Karl M Kadish, Kevin M Smith, Roger Guilard, eds.). World Scientific Publishing; 2019.
- Loas A, Gerdes R, Zhang Y and Gorun SM. *Dalton Trans.* 2011; **40**: 5162–5165.
- Carrión EN, Loas A, Patel HH, Pelmuş M, Ramji K and Gorun SM. *J. Porphyrins Phthalocyanines* 2018; **22**: 371–397.
- Pinnock J, Hansen K, Pelmuş M and Fadeev AY. *Langmuir* 2025; **41**: 8202–8213.
- Neven L, Barich H, Ching HYV, Khan SU, Colomier C, Patel HH, Gorun SM, Verbruggen S, Van Doorslaer S and De Wael K. *Anal. Chem.* 2022; **94**: 5221–5230.
- Patel HH. Fluorinated Metallo Phthalocyanines for Chemical and Biological Catalysis. Ph.D. Thesis, Seton Hall University, South Orange, NJ 07079, 2015.
- Szczubialka K, Łapok Ł, Skiba M, Patel H, Gorun SM, Nowakowska M and Drozd D. *Appl. Catal. B-Environ.* 2012; **125**: 35–40.
- Bushnaq H, Munro C, Pu S, Razmjou A, Zargar M, Palmisano G, Mettu S and Dumée LF. *J. Water Process Eng.* 2024; **65**: 105861.
- Bench BA, Brennessel WW, Lee H-J and Gorun SM. *Angew. Chem., Int. Ed.* 2002; **41**: 750–754.
- Brinkmann H, Kelting C, Makarov S, Tsaryova O, Schnurpfeil G, Wöhrle D and Schlettwein D. *Phys. Status Solidi A*. 2008; **205**: 409–420.
- Nagel S, Lener M, Keil C, Gerdes R, Łapok Ł, Gorun SM and Schlettwein D. *J. Phys. Chem. C* 2011; **115**: 8759–8767.
- Trashin S, Rahemi V, Ramji K, Neven L, Gorun SM and De Wael K. *Nature Commun.* 2017; **8**: 16108.
- Bench BA, Beveridge A, Sharman WM, Diebold GJ, van Lier JE and Gorun SM. *Angew. Chem., Int. Ed.* 2002; **41**: 773–776.
- Zheng F, Huang Y, Shen Y, Chen G, Peng Y and Zhuang X. *Photodiagnosis Photodyn. Ther.* 2023; **43**: 103734.
- Gouterman M. *J. Mol. Spectrosc.* 1961; **6**: 138–163.
- Gouterman M. Porphyrins: Excited States and Dynamics. Vol. 321. ACS Symposium Series. (Rentzepis PM, Gouterman M, Straub KD, eds.). American Chemical Society; 1986.
- Gouterman M. In D. Dolphin, ed. The Porphyrins: Physical Chemistry. Vol. 3 Part A. Part 1. Academic Press, 1979; 1–165.
- Kobayashi N, Muranaka A and Mack J. In Kobayashi N, Muranaka A, Mack J, eds. Circular Dichroism and Magnetic Circular Dichroism Spectroscopy for Organic Chemists. The Royal Society of Chemistry, 2011; 172–191.
- Yamamoto S, Zhang A, Stillman MJ, Kobayashi N and Kimura M. *Chem. Eur. J.* 2016; **22**: 18760–18768.
- Mack J, Asano Y, Kobayashi N and Stillman M. *J. Am. Chem. Soc.* 2005; **127**: 17697–17711.
- Pelmuş M, Carrión EN, Colomier C, Santiago J and Gorun SM. *J. Porphyrins Phthalocyanines* 2016; **20**: 1401–1408.
- Keizer SP, Mack J, Bench BA, Gorun SM and Stillman MJ. *J Am Chem Soc* 2003; **125**: 7067–7085.
- Liao MS, Watts JD, Huang MJ, Gorun SM, Kar T and Scheiner S. *J. Chem. Theory Comput.* 2005; **1**: 1201–1210.
- Liao MS, Kar T, Gorun SM and Scheiner S. *Inorg. Chem.* 2004; **43**: 7151–7161.
- Gaussian 16, Revision B.01, Frisch MJ, Trucks GW, Schlegel HB, Scuseria GE, Robb MA, Cheeseman JR, Scalmani G, Barone V, Petersson GA, Nakatsuji H, Li X, Caricato M, Marenich AV, Bloino J, Janesko BG, Gomperts R, Mennucci B, Hratchian HP, Ortiz JV, Izmaylov AF, Sonnenberg JL, Williams-Young D, Ding F, Lipparini F, Egidi F, Goings J, Peng B, Petrone A, Henderson T, Ranasinghe D, Zakrzewski VG, Gao J, Rega N, Zheng G, Liang W, Hada M, Ehara M, Toyota K, Fukuda R, Hasegawa J, Ishida M, Nakajima T, Honda Y, Kitao O, Nakai H, Vreven T, Throssell K, Montgomery Jr. JA, Peralta JE, Ogliaro F, Bearpark MJ, Heyd JJ,

- Brothers EN, Kudin KN, Staroverov VN, Keith TA, Kobayashi R, Normand J, Raghavachari K, Rendell AP, Burant JC, Iyengar SS, Tomasi J, Cossi M, Miller JM, Klene M, Adamo C, Cammi R, Ochterski JW, Martin RL, Morokuma K, Farkas O, Foresman JB and Fox DJ. Gaussian, Inc., Wallingford, CT, 2016, GaussView 5.0. Wallingford, E.U.A.
27. Nemykin VN, Hadt RG, Belosludov RV, Mizuseki H and Kawazoe Y. *J. Phys. Chem. A* 2007; **111**: 12901–12913.
 28. Nyokong T, Gasyna Z and Stillman MJ. *Inorg. Chem.* 1987; **26**: 1087–1095.
 29. Bunin DA, Martynov AG, Gvozdev DA and Gorbulanova YG. *Biophys Rev* 2023; **15**: 983–998.
 30. Piepho SB and Schatz PN. In Group Theory in Spectroscopy with Applications to Magnetic Circular Dichroism. New York: Wiley-Interscience Monographs in Chemical Physics, John Wiley, 1983; 58–97.
 31. Scheidt WR and Dow W. *J. Am. Chem. Soc.* 1977; **99**: 1101–1104.
 32. Jiang H, Ye J, Hu P, Wei F, Du K, Wang N, Ba T, Feng S and Kloc C. *Sci. Re.* 2014; **4**: 7573.
 33. Loas AI. Rational design of hydrogen-free catalytic active sites. Ph. D. Thesis, New Jersey Institute of Technology, Newark, NJ 07102, 2012.
 34. Stillman MJ and Nyokong T. In Leznoff CC, Lever ABP, eds. Absorption and Magnetic Circular Dichroism Spectral Properties of Phthalocyanines. Vol. 1. New York: VCH Publishers, Inc, 1989; 133–289.
 35. Dwyer PJ, Vander Valk RJ, Caltaldo V, Demianicz D and Kelty SP. *J. Phys. Chem. A* 2014; **118**: 11583–11590.
 36. Moons H, Patel HH, Gorun SM and Van Doorslaer S. *Z. Phys. Chem.* 2017; **231**: 887–903.
 37. Liao M-S, Watts JD, Gorun SM, Scheiner S and Huang M-J. *J. Chem. Theory Comput.* 2008; **07**: 541–563.
 38. Faraonov MA, Yakushev IA, Yudanova EI, Pelmus M, Gorun SM, Otsuka A, Yamochi H, Kitagawa H and Konarev DV. *Inorg. Chem.* 2023; **62**: 11390–11401.